

# Unsupervised Real-World Denoising: Sparsity is All You Need

Hamadi Chihaoui   Paolo Favaro  
 Computer Vision Group, University of Bern, Switzerland  
 {hamadi.chihaoui, paolo.favaro}@unibe.ch

## Abstract

Supervised training for real-world denoising presents challenges due to the difficulty of collecting large datasets of paired noisy and clean images. Recent methods have attempted to address this by utilizing unpaired datasets of clean and noisy images. Some approaches leverage such unpaired data to train denoisers in a supervised manner by generating synthetic clean-noisy pairs. However, these methods often fall short due to the distribution gap between synthetic and real noisy images. To mitigate this issue, we propose a solution based on input sparsification, specifically using random input masking. Our method, which we refer to as *Mask, Inpaint and Denoise (MID)*, trains a denoiser to simultaneously denoise and inpaint synthetic clean-noisy pairs. On one hand, input sparsification reduces the gap between synthetic and real noisy images. On the other hand, an inpainter trained in a supervised manner can still accurately reconstruct sparse inputs by predicting missing clean pixels using the remaining unmasked pixels. Our approach begins with a synthetic Gaussian noise sampler and iteratively refines it using a noise dataset derived from the denoiser’s predictions. The noise dataset is created by subtracting predicted pseudo-clean images from real noisy images at each iteration. The core intuition is that improving the denoiser results in a more accurate noise dataset and, consequently, a better noise sampler. We validate our method through extensive experiments on real-world noisy image datasets, demonstrating competitive performance compared to existing unsupervised denoising methods.

## 1. Introduction

Image denoising is one of the most long-studied problems in computer vision, thanks to its fundamental formulation that makes it the first step in testing image processing methods, as well as the realization that denoisers can serve multiple purposes [9]. Traditional denoising methods rely on supervised learning, where pairs of clean and noisy images are available for training. However, in real-world scenarios,

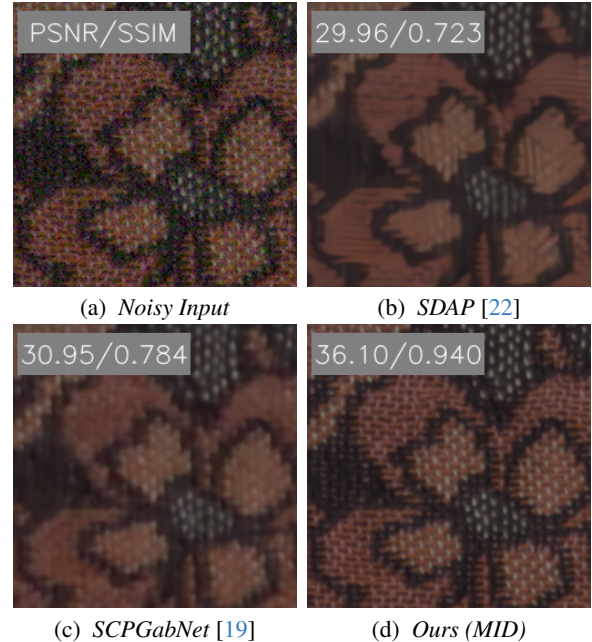


Figure 1. Visual comparison of unsupervised denoising methods on the SIDD validation dataset. Our method (MID) preserves fine details better. Zoom in to see the reconstruction accuracy.

acquiring paired noisy-clean image datasets is often impractical. This has led to significant interest in unsupervised image denoising techniques, particularly in unpaired settings, where unrelated noisy and clean images (with no pairing) are available.

One intuitive approach is to use an Additive White Gaussian Noise (AWGN) sampler to generate a paired dataset of noisy-clean images and train a denoiser in a supervised manner. However, the mismatch between the synthetic noise distribution and real-world noise leads to poor performance at test time. In alternative, several unsupervised methods have also been proposed for the unpaired setting. These methods aim to learn or approximate the real noise distribution through adversarial training, typically involving a generative model and a discriminator. However, such

methods often suffer from training instability and mode collapse, limiting their ability to effectively estimate real-world noise. This is due to the complexity and unknown nature of real-world noise distributions, often presenting local correlations.

In this work, we explore a novel approach that *removes the need for adversarial training* and bridges the gap between synthetic and real-world noise. We propose jointly training a denoiser to perform both denoising and inpainting on sparse inputs by using an AWGN sampler with random input masking to generate a synthetic paired dataset of noisy-clean images. *Our key idea is that randomly masking parts of both synthetic noisy images during training and real noisy images during testing reduces the distribution gap between training and testing phases.* The missing content caused by masking can still be recovered by training the denoiser to inpaint the input simultaneously, leveraging the remarkable capabilities of deep neural networks and the inherent redundancy of natural images. Once the initial denoiser is trained, we propose a framework that iteratively refines the noise sampler by using the denoiser to generate a dataset of pseudo real-world noise. We show that by repeating this procedure iteratively, we can gradually improve the noise sampler and, more importantly, achieve a better-performing denoiser. We incorporate these insights into a novel method called Mask, Inpaint and Denoise (MID), which we elaborate on further in Sec. 3 and illustrate in Figure 2. In comparison to state-of-the-art unsupervised denoising methods, MID behaves favorably in terms of both quantitative metrics and perceptual quality (see, for example, Figure 1).

Our contributions are summarized as follows

- We introduce Mask, Inpaint and Denoise (MID), an innovative unsupervised image denoising method that utilizes random input masking to bridge the gap between the training phase (synthetic noise) and the testing phase (real noise). By randomly masking portions of the noisy image during both training and testing, we reduce the distribution mismatch between synthetic and real noise, enhancing the generalization ability of the denoiser to real-world noisy images without requiring paired noisy-clean datasets.
- To the best of our knowledge, we are the **first** to apply random input masking in the context of unpaired image denoising, eliminating the need for adversarial training and its associated limitations.
- We propose an iterative procedure to refine noise samplers using residual noise from denoised real images. By progressively improving the sampler, our method enhances the denoiser’s performance and adaptability to real noise.
- MID outperforms all unsupervised methods in the unpaired setting and is on par or better than the other unsu-

pervised methods in real-world denoising across multiple datasets.

## 2. Related Work

### 2.1. Non-learning-based image denoisers

Traditional denoising algorithms, such as those found in [4, 26, 33], define clean image properties using manually crafted priors. Some methods emphasize sparse representations [2, 20], whereas others exploit the inherent recurrence of image patches [34]. BM3D [7], which employs collaborative filtering across similar image patches, is widely recognized for its strong performance on various benchmarks. Similarly, methods like NLM [3] and WNNM [25] also rely on leveraging related patches, using an implicit averaging strategy to reduce noise effectively.

### 2.2. Supervised Image Denoising

Supervised image denoising methods [30–32] train a neural network using a paired dataset of noisy images. [32] proposes a residual learning-based deep convolutional neural network (CNN) for image denoising, going beyond traditional Gaussian denoisers. By focusing on learning residual noise instead of directly predicting the clean image, the method effectively enhances denoising performance. [30] focuses on blind noise modeling and removal by leveraging a variational inference framework. It jointly learns noise distributions and denoises images, enabling the network to adapt to various types and levels of noise. Restormer [31] introduces an efficient transformer-based architecture specifically designed for high-resolution image restoration tasks. By leveraging multi-head self-attention mechanisms within a window-based framework, it achieves computational efficiency and superior performance. However, these methods rely on paired datasets, which may be expensive to acquire, thus limiting their applicability in practice.

### 2.3. Unsupervised Image Denoising

**Self-Supervised Image Denoising** Self-supervised denoising methods train a denoiser using only a dataset of noisy images. Noise2Void [12] employs a masking strategy to split noisy images into input-target pairs. Blind-spot networks further enhance this approach by removing the corresponding noisy pixel from the input’s receptive field for each output pixel. To address information loss in the blind spot, probabilistic inference [13, 15] and regularization loss functions [27] have been introduced. However, these self-supervised approaches are often limited to noise that is spatially independent. Some methods have also aimed to remove spatially correlated noise in a self-supervised manner. CVF-SID [21] separates noisy images into clean image and noise components. Among self-supervised approaches for real-world sRGB noise, AP-BSN [16] proposes asym-

metric PD factors and post-refinement processing to better balance noise removal and aliasing artifacts, though it is computationally intensive during inference. SDAP [22] generates random sub-samples from noisy images to create pseudo-clean targets, avoiding the need for paired clean-noisy datasets. LG-PBN [28] improves denoising by combining local and global patch-level features, using a blind-patch strategy to handle diverse noise patterns effectively in real-world images. Li et al. [17] introduce a spatially adaptive self-supervised learning method for real-world image denoising, where the model dynamically adjusts to different noise levels across image regions. AT-BSN [6] employs efficient asymmetric blind-spots in self-supervised denoising to enhance performance in real-world scenarios. However, those methods may be suboptimal from an information perspective, as they do not take advantage of the abundance of noise-free dataset [8, 14, 18] available in the digital world.

**Unpaired Image Denoising** Unpaired methods [10, 19, 29] address the challenge of data collection by training networks on datasets containing unpaired noisy and clean images. Many of these methods [10, 19, 29] focus on learning noise characteristics through adversarial training. This involves initially training a noise generator to replicate the noise distribution observed in noisy images, which is then used to transform clean images into synthetic noisy versions. The denoising network is subsequently trained using these synthetic noisy-clean image pairs. Additionally, Wu et al. [29] adopt a joint approach by training both a denoising network and a noise estimator simultaneously to model the noise distribution. The final denoising network is trained with a combination of synthetic noisy-clean pairs and noisy-denoised image pairs. Despite these efforts, accurately modeling noise distribution in the complex sRGB space remains challenging, limiting the effectiveness of unpaired methods for real-world photographs. SCPGabNet [19] introduce an unsupervised approach to image denoising using two parallel generative adversarial branches that collaborate to reduce noise. These branches exchange and refine information, enabling the model to clean noisy images without requiring matched noisy-clean data pairs. Our method falls within this category. Unlike previous works, MID: 1) removes the need for adversarial training, 2) proposes a novel integration of masking with supervised training using synthetic noise, and 3) starts with a Gaussian noise sampler and iteratively refines it. To the best of our knowledge, these contributions have not been presented before.

### 3. Unsupervised Image Denoising using MID

In this work, we assume access to a dataset of *unpaired* noisy  $\mathcal{Y} = \{y_1^r, \dots, y_n^r\}$  and clean images  $\mathcal{X} = \{x_1, \dots, x_c\}$ . In general,  $y^r \in \mathcal{Y}$  denotes one of the images corrupted with real noise, while  $x \in \mathcal{X}$  represents one of

the clean images. In our approach  $x$  and  $y^r$  are not paired, that is,  $y^r$  is a noisy image that has nothing to do with the clean image  $x$ . Our goal is to train a denoiser in a fully unsupervised manner by relying on these two datasets. In this section, we present our unsupervised denoising method MID in detail.

#### 3.1. Limitations of Supervised Learning with Synthetic Data

One approach in the unpaired setting is to generate synthetic noisy-clean image pairs by adding synthetic noise to the clean images  $x$  and then by training a denoiser in a supervised manner. A simple choice to obtain noise samples is to use an Additive White Gaussian Noise (AWGN) sampler. To increase the computational efficiency, we draw a finite set of AWGN samples only once and then collect them in the set  $\mathcal{N}_0$ . Then, at training time, whenever we need a new synthetic noise sample, we randomly select an element  $n^s \sim \mathcal{N}_0$ . Formally, given a clean image  $x$ , the corresponding synthetic noisy image is generated via  $y^s = x + n^s$ . A denoiser  $\mathcal{D}_0^s$  can then be trained by minimizing

$$\min_{\mathcal{D}_0^s} \sum_{x \in \mathcal{X}, n^s \sim \mathcal{N}_0} \|\mathcal{D}_0^s(x + n^s) - x\|^2. \quad (1)$$

The main shortcoming of this approach is that such a denoiser tends to perform poorly at test time, when applied to real-world noisy images  $y^r$ . This is due to the fact that during training the input is  $y^s = x + n^s$ , whereas at test time, the input is  $y^r = x + n^r$ . Unless real noise is AWGN,  $n^r$  and  $n^s$  will have different distributions and thus  $y^r$  will be out of distribution for  $\mathcal{D}_0^s$ . As shown in Figure 3, a denoiser trained on clean images from the SIDD medium dataset with AWGN and applied to real noisy images from the SIDD validation dataset yields a poor performance.

#### 3.2. Input Sparsification for Bridging the Synthetic-Real Distribution Gap

To improve the performance of a denoiser trained on synthetic noisy-clean images, it is essential to minimize the distribution gap between the training (synthetic data) and testing (real data) phases. We propose a novel method to achieve this. We propose reducing the train-test distribution gap by randomly masking the noisy inputs during both training and testing. We train the denoiser  $\mathcal{D}_0$  by minimizing

$$\min_{\mathcal{D}_0} \sum_{\substack{x \in \mathcal{X}, n^s \sim \mathcal{N}_0 \\ y^s = x + n^s, \mathbf{M} \sim \mathcal{M}_\alpha}} \|\mathcal{D}_0(\mathbf{M} \odot y^s) - x\|^2, \quad (2)$$

where  $\mathbf{M} \sim \mathcal{M}_\alpha$  is a binary random mask sample,  $\mathcal{M}_\alpha$  is the set of all masks with the given masking ratio  $\alpha$  (in practice, we do not use a finite set, but randomly sample from a Bernoulli distribution at each pixel), and  $\odot$  denotes the

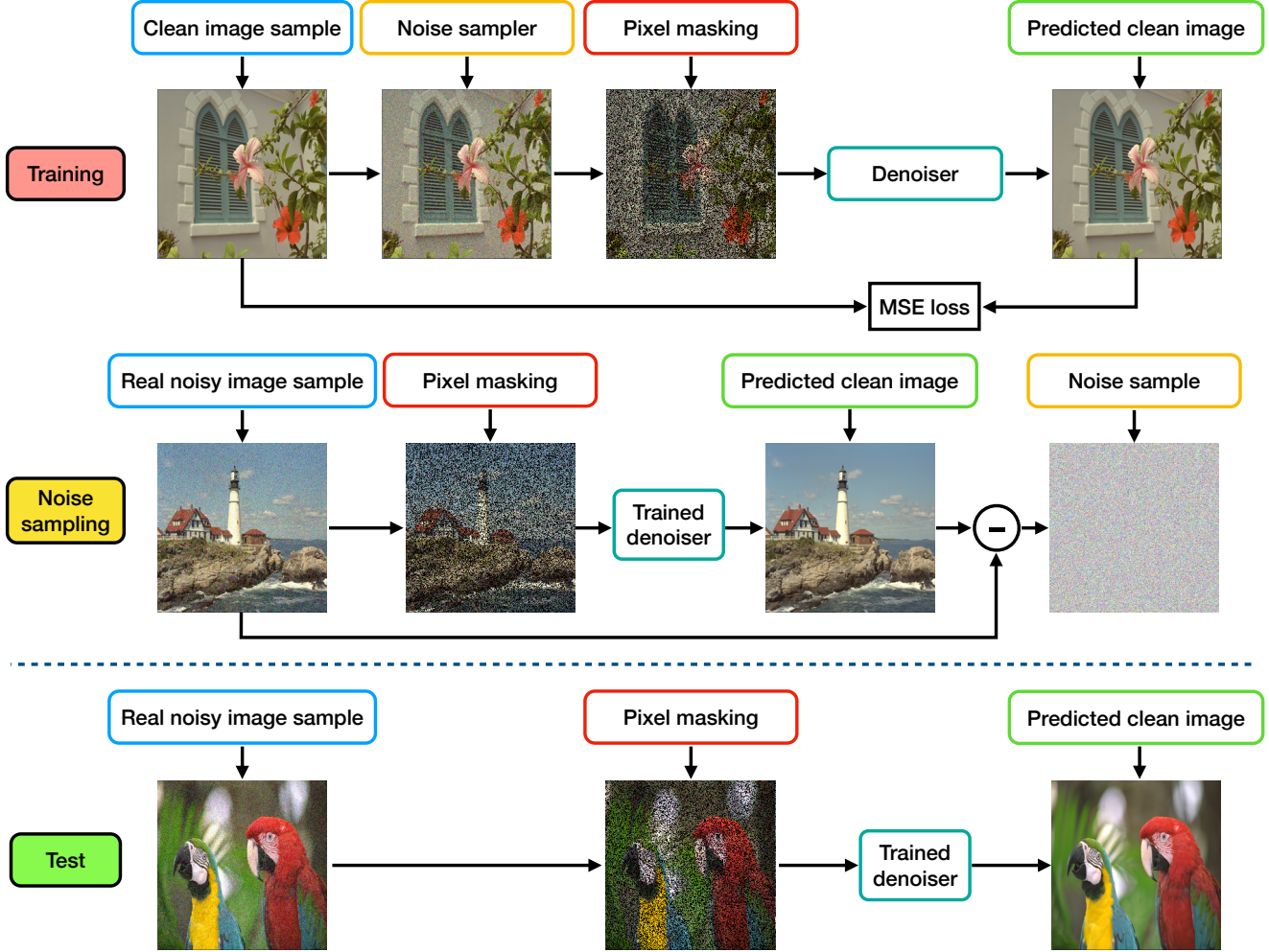


Figure 2. Overview of MID. Top row: We show the processing steps used during supervised training. We use clean images from the available dataset, add synthetic noise (initially simply AWGN, and then later the noise samples are extracted from the real noisy images), mask the pixels and then train a denoiser to predict the clean image by minimizing a Mean Squared Error (MSE) loss. Middle row: To obtain better noise samples, we use the trained denoiser on the dataset of real noisy images. The noise samples are obtained simply by computing the residual between the predicted pseudo-clean image and the original noisy input. These residuals are then used as new noise samples in a new training of the denoiser. Bottom row: At test time we simply apply the trained denoiser on new real noisy images after applying masking. To further boost the accuracy, we average the predicted clean images for several random masks.

Hadamard element-wise (per pixel) product. This training involves simultaneously learning to denoise and to inpaint, and that is why we call our method Mask, Inpaint and Denoise, or in short, MID. At test time, the denoiser is also applied to  $\mathbf{M} \odot y^r = \mathbf{M} \odot (x + n^r)$ .

Input masking reduces the distribution gap between the synthetic training inputs and the real testing inputs. A formal proof is provided in Section A of the appendix. Intuitively, masking synthetic noisy images during training and real noisy images during testing increases the shared content between them (i.e., the masked pixels). In the extreme case where all pixels are masked ( $\mathbf{M} = \mathbf{0}$ ), the two distri-

butions become identical.

While input masking helps bridge the gap between synthetic and real-world noisy images, it can, however, negatively impact the training of the denoiser (which performs both denoising and inpainting simultaneously) by removing valuable input information. In fact, excessive masking may make the inpainting task overly ambiguous, leading to a poorly trained denoiser. This raises the question of how well an inpainter trained with randomly masked pixels can generalize to new images. In the next subsection, we address this aspect by examining the effect of the input masking ratio on the inpainter performance through experimental

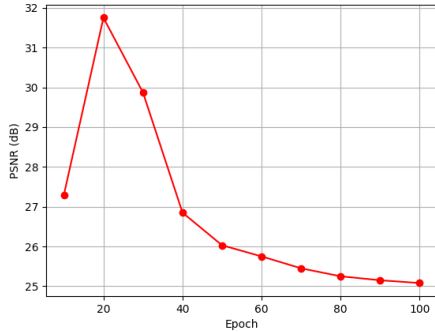


Figure 3. The denoiser performance on SIDD validation set when trained with an AWGN sampler.

analysis.

### 3.3. Achieving Accurate Reconstruction of Sparse Inputs with Supervised Inpainting

We analyze the performance of an inpainter trained to reconstruct masked portions of an input image (*i.e.*, the inpainter learns the mapping  $\mathbf{M} \odot x \rightarrow x$  - *i.e.*, no denoising) under different masking ratios between 20% and 90%. Since we are interested in the exact reconstruction of the original image (*i.e.*, before masking), we evaluate the inpainted one based on how accurately the output image matches the original image. To achieve this, we train an inpainter using the Imagenet validation dataset, where 90% of the dataset is used for training and the remaining 10% serves as a held-out test/validation set. The inpainter is trained to recover the masked pixels using the Mean Squared Error (MSE) loss via supervised learning.

We assess the inpainter’s performance on the held-out validation dataset during training. Figure 4 illustrates the PSNR values of the inpainted images, comparing them to the original images on the validation set as a function of the masking ratio. We observe that the performance of the inpainter decreases with higher masking ratios. This is to be expected, as the task difficulty (and ambiguities) grow proportionally to the masking ratio. Nonetheless, even at an 80% masking ratio a reconstruction PSNR above 35dB is excellent. Figure 5 also shows the reconstruction of images when 80% of the input pixels are masked. This surprisingly positive outcome can be explained by 1) the redundancy of information in natural images, which enables the inpainter to accurately predict masked pixels based on the observed ones, as well as 2) the advancement of Deep Neural Networks architectures and training.

By combining (1) the findings from Sec. 3.2, which show that random pixel masking reduces the gap between training and testing inputs, with (2) the experiments in Figure 4, which demonstrate that a high masking ratio does not hinder

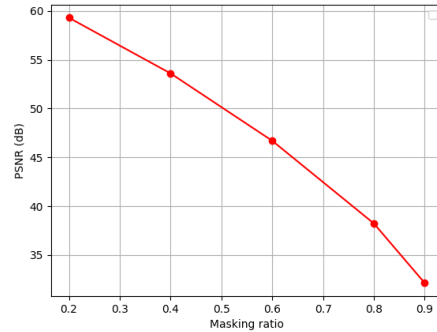


Figure 4. Inpainter performance on a validation set trained in a supervised way at different random masking ratios.

the reconstruction of missing clean data due to the strong correlations in natural images, we suggest that a denoiser can be more effectively trained to jointly denoise and inpaint synthetic noisy-clean images while applying random input masking to the noisy data. Once trained, the denoiser can be leveraged to obtain a better noise sampler by subtracting predicted pseudo-clean images from real noisy images. This process creates a virtuous cycle, where a denoiser trained in this manner benefits from synthetic noise samples that are more realistic (*i.e.*, closer to real noise) than those used during its initial training. Consequently, a new denoiser trained on these improved samples can achieve even better denoising performance.

### 3.4. Iterative Noise Sampler Boosting

In this section, we assume to start with a well-trained denoiser ( $\mathcal{D}_0$ ) and explore the idea of iteratively refining a noise sampler to progressively better match the real noise distribution.

We obtain pseudo-real noise samples by applying the denoiser  $\mathcal{D}_0$  to the set of real noisy images  $y^r \in \mathcal{Y}$  after applying random masking. We compute the pseudo-real noise samples as the difference between the noisy image  $y^r$  and the predicted denoised images  $\mathcal{D}_0(\mathbf{M} \odot y^r)$ , with  $\mathbf{M} \sim \mathcal{M}_\alpha$ . We define the set of pseudo-real noise samples as  $\mathcal{N}_1 \doteq \{y^r - \mathcal{D}_0(\mathbf{M} \odot y^r), \forall y^r \in \mathcal{Y} \text{ and } \mathbf{M} \sim \mathcal{M}_\alpha\}$ .

If we had an accurate denoiser we would obtain a set of pseudo-real noise samples  $\mathcal{N}_1$  that would fit well the distribution of real-world noise. Vice versa, if we used real-world noise as synthetic noise in the training of the denoiser, we would obtain a denoiser that would generalize very well on real noise images. MID addresses this chicken and egg problem by using an iterative procedure that builds a positive gain over iteration time. At iteration  $k$ , MID adds randomly selected pseudo-real noise samples from  $n^p \in \mathcal{N}_k$  to the clean images  $x$ , randomly masks them with a binary mask  $\mathbf{M} \sim \mathcal{M}_\alpha$ , and then trains the denoiser  $\mathcal{D}_k$  to predict

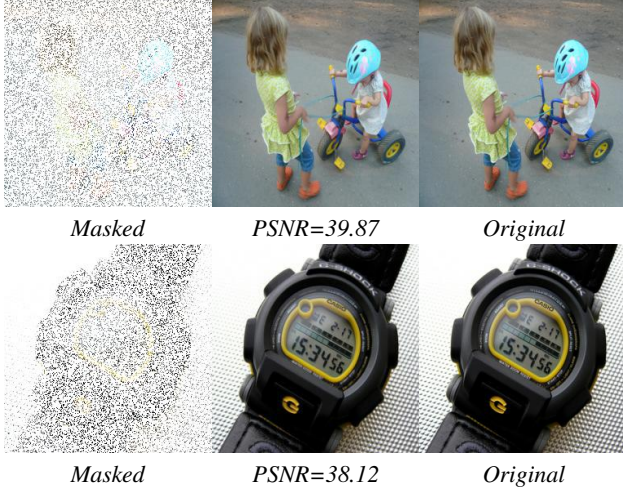


Figure 5. Left: Masked input at 80% of the pixels. Middle: The output of the inpainter on the image on the left. Right: Original images from the validation set.

$x$  from  $\mathbf{M} \odot (x + n^p)$  by solving

$$\min_{\mathcal{D}_k} \sum_{\substack{x \in \mathcal{X}, n^p \sim \mathcal{N}_k, \\ \mathbf{M} \sim \mathcal{M}_\alpha}} \|\mathcal{D}_k(\mathbf{M} \odot (x + n^p)) - x\|. \quad (3)$$

The pseudo-real noise set  $\mathcal{N}_k$  is then computed as

$$\mathcal{N}_k = \{y^r - \mathcal{D}_{k-1}(\mathbf{M} \odot y^r), \forall y^r \in \mathcal{Y}, \mathbf{M} \sim \mathcal{M}_\alpha\}, \quad (4)$$

except for the initial set  $\mathcal{N}_0$ , which consists of AWGN samples. As shown in the experiments, although we start with AWGN samples, thanks to masking, the denoiser is able to generalize well on real noisy images and to yield a set of pseudo-real noise samples  $\mathcal{N}_1$  that is better than AWGN. We see experimentally that the noise samples  $\mathcal{N}_k$  become more and more realistic over time, as the denoiser  $\mathcal{D}_k$  improves its generalization performance over iteration time  $k$ .

### 3.5. Mask, Inpaint and Denoise

By putting all the previous steps together we can present our method for unsupervised image denoising in the unpaired data setting. We start with a cost-effective sampler  $\mathcal{N}_0$ , *e.g.*, an AWGN sampler, and use it to train a denoiser. The denoiser is then applied iteratively to generate a better noise sampler, as described in the previous section, which in turn improves the denoiser. The steps for MID are summarized in Algorithm 1. At test time, given a real-world noisy image  $y^r$ , the recovered clean image  $\hat{x}$  is obtained as an ensemble of  $K$  predictions

$$\hat{x} = \frac{1}{K} \sum_{p=1, \mathbf{M} \sim \mathcal{M}_\alpha}^K \mathcal{D}_m(\mathbf{M} \odot y^r), \quad (5)$$

where for each prediction, a random binary mask  $\mathbf{M}$  is sampled and applied to the input image.

---

### Algorithm 1 MID

---

**Require:** Unpaired noisy  $\mathcal{Y}$  and clean  $\mathcal{X}$  datasets, total number of iterations  $m$ .

**Ensure:** Final denoising model  $\mathcal{D}_m$

- 1: Initialize the noise samples set  $\mathcal{N}_0$  with AWGN samples.
  - 2: **for**  $k = 0$  **to**  $m$  **do**
  - 3:   Train a denoiser  $\mathcal{D}_k$  by minimizing Eq. (3)
  - 4:   Build the noise sample set  $\mathcal{N}_k$  as in Eq. (4)
  - 5: **end for**
  - 6: Return denoising model  $\mathcal{D}_m$
- 

## 4. Experiments

In this section, we will first introduce the experimental settings. We will then present the quantitative and qualitative results of MID, along with comparisons with other methods.

### 4.1. Experimental settings

**Training and test data.** To train our method, we use the SIDD [1] Medium training set (which contains 320 pairs of noisy images and corresponding clean images captured using various smartphones). We begin by equally splitting the SIDD Medium training set into separate noisy and clean image groups. From this split, we use 160 clean images from one group and 160 noisy images from the other to create an unpaired dataset of real images for training the proposed algorithm. We evaluate our method using three widely recognized real-world noisy datasets: the SIDD [1] Validation set, SIDD [1] Benchmark, and the DND [23] Benchmark. It is worth noting that the denoised images from the SIDD Benchmark and DND Benchmark can be uploaded to their respective websites to obtain PSNR and SSIM results. Unfortunately, the SIDD platform is currently unavailable and has been replaced by a Kaggle competition, which does not yet contain all the data. We reported our results and marked the entries with <sup>†</sup>. Additionally, we included some other unsupervised methods that have publicly shared their trained models to ensure a fairer comparison. It is also important to note that SSIM values may be calculated differently; the values reported by the Kaggle leaderboard reflect this variation. One explanation is that computing SSIM in the range [0, 1] versus [0, 255] can lead to significant differences in results.

**Implementation details.** The network architecture for MID follows the same structure as in NAFNet [5]. We train the denoiser for four rounds: the first round uses AWGN noise, while the remaining three rounds utilize residual noise derived from the last trained denoiser. For the masking ratio, we initially start at 80% and then decrease it to 70%. In the final round (when the denoiser is expected to perform better), we use a range of [50%, 70%]. It is im-

Table 1. Quantitative comparisons (PSNR(dB) and SSIM) of MID and other real-world denoising methods on SIDD and DND datasets. The best results of the unsupervised approaches are marked in **bold**, while the second best ones are underlined.

Category	Method	SIDD Validation		SIDD Benchmark		DND Benchmark	
		PSNR $\uparrow$	SSIM $\uparrow$	PSNR $\uparrow$	SSIM $\uparrow$	PSNR $\uparrow$	SSIM $\uparrow$
Non-learning based	BM3D [7]	25.71	0.576	25.65	0.685	34.51	0.851
	WNNM [11]	26.05	0.592	25.78	0.809	34.67	0.865
Supervised (Real pairs)	DnCNN [32]	37.73	0.943	37.61	0.941	38.73	0.945
	Baseline, N2C [24]	38.98	0.954	38.92	0.953	39.37	0.954
	VDN [30]	39.29	0.956	39.26	0.955	39.38	0.952
	Restormer [31]	39.93	0.960	40.02	0.960	40.03	0.956
Self-Supervised	CVF-SID [21]	34.15	0.911	34.71	0.917	36.50	0.924
	AP-BSN+R <sup>3</sup> [16]	36.74	0.934	36.91	0.931	38.09	0.937
	Li et al. [17]	37.39	0.934	<u>37.41</u>	0.934	38.18	0.938
	LG-BPN [28]	-	-	37.28	0.936	<b>38.43</b>	<b>0.942</b>
	SDAP [22]	37.30	0.939	37.24/37.79 <sup>†</sup>	0.936/0.886 <sup>†</sup>	37.86	0.937
	AT-BSN [6]	<u>37.88</u>	<u>0.942</u>	<b>37.77</b>	<b>0.946</b>	38.29	0.939
Unpaired	Wu et al. [29]	-	-	-	-	37.93	0.937
	C2N [10]	35.36	0.932	35.35	<u>0.937</u>	37.28	0.924
	SCPGabNet [19]	36.53	-	36.53/36.98 <sup>†</sup>	0.925/0.875 <sup>†</sup>	38.11	<u>0.939</u>
	Ours (MID)	<b>38.05</b>	<b>0.949</b>	<b>38.03</b> <sup>†</sup>	<b>0.906</b> <sup>†</sup>	<u>38.38</u>	<b>0.942</b>

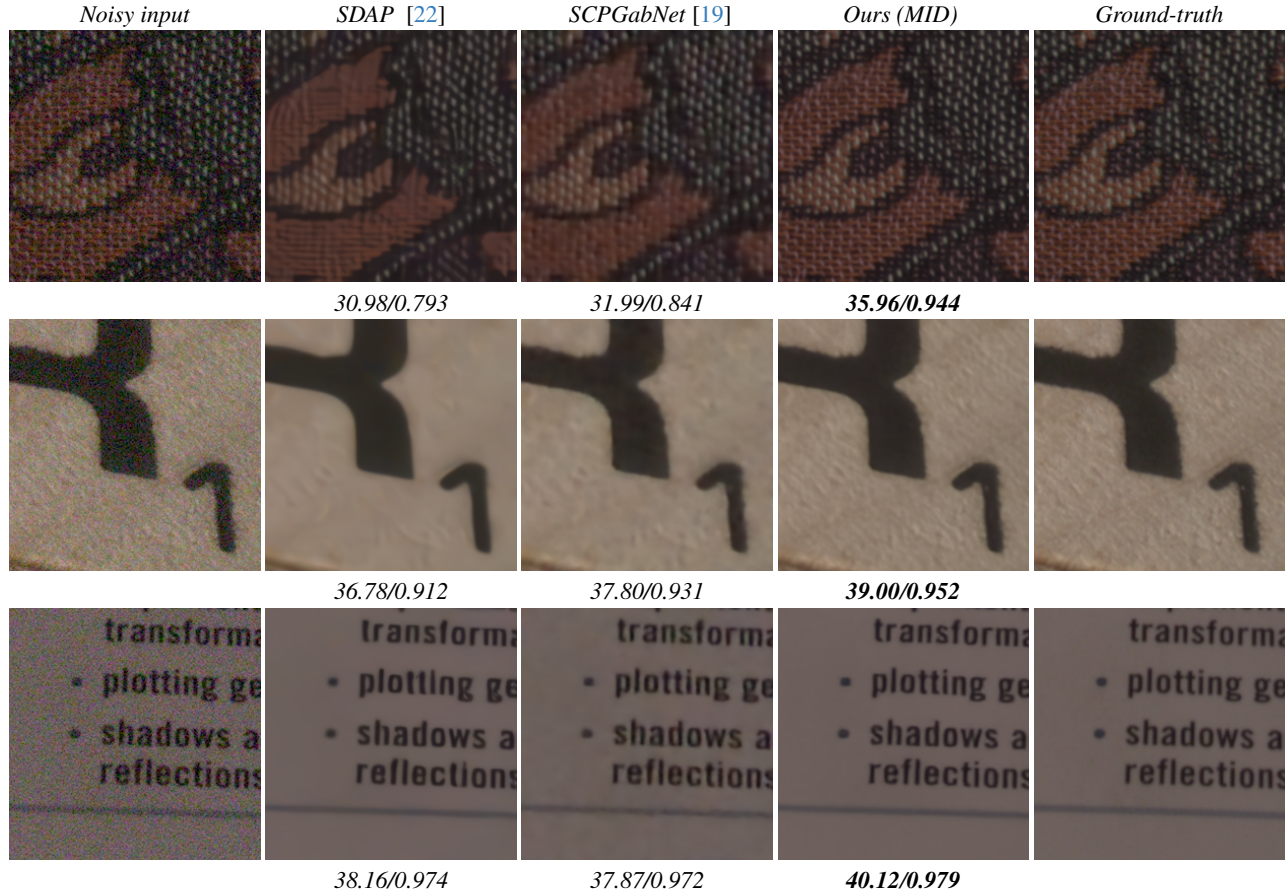


Figure 6. Visual comparison on SIDD validation dataset. Zooming in is recommended to see the differences in reconstruction accuracy.

portant to note that the denoiser is retrained from scratch at each stage. The final denoised image is an ensemble of

$K = 10$  predictions. The denoising network is trained from scratch for  $2 \cdot 10^5$  iterations using the Adam optimizer with

Table 2. Effect of the Denoiser architecture for MID on the SIDD validation dataset.

Denoiser Architecture	PSNR $\uparrow$	SSIM $\uparrow$
DnCNN [32]	36.85	0.934
NAFNet [5]	<b>38.05</b>	<b>0.949</b>

Table 3. Effect of the iterative noise sampler boosting method in MID on the SIDD validation dataset.

Round Number	1	2	4	6
PSNR	36.38	37.43	38.05	37.96

Table 4. Effect of each component of MID on the SIDD validation dataset.

Method	PSNR
w/o masking	25.24
w/o iterative refinement	36.38
w/o prediction ensembling	37.68
Ours	<b>38.05</b>

Table 5. Effect of the number  $K$  of MID predictions used in the ensemble on the SIDD validation dataset.

$K$	1	5	10	20
PSNR	37.68	37.87	38.05	38.07

Table 6. Effect of the masking ratio in the first round of MID (AWGN denoising) on the SIDD validation dataset.

Masking ratio	0%	40%	60%	80%	90%
PSNR	25.24	34.12	35.65	<b>36.38</b>	35.90

initial learning rate of  $4 \cdot 10^{-4}$  and decayed to  $10^{-6}$  using a cosine annealing scheduler.

**Quantitative Comparison.** Table 1 presents the quantitative comparison results for the SIDD and DND datasets. Our approach outperforms all existing unpaired methods [10, 19, 29] by a significant margin of approximately 1.3 dB on the SIDD dataset. For self-supervised methods, MID is on par or slightly better than the state-of-the-art AT-BSN [6] and clearly outperforms all other self-supervised methods. When note that AT-BSN is a distillation-based method that trains multiple denoisers before distilling them while our method train a single network. When evaluated using PSNR and SSIM metrics, our method achieves performance levels comparable to DnCNN [32], which has been trained on real-world paired datasets.

**Qualitative Comparison.** The visual comparison of state-of-the-art self-supervised methods on the benchmark datasets is shown in Figure 7. MID generates more detailed image compared to other methods.

## 5. Ablation Study

We conduct extensive ablation studies on SIDD validation dataset to analyze the effectiveness of each component of MID.

### 5.1. Effect of each component of MID

In Table 4, we quantify the effect of the components of MID: input masking, iterative refinement of the noise sampler, and prediction averaging. Masking is crucial, as training ends with overfitting without it. The iterative refinement of the noise sampler contributes around 1.7 dB to the final performance, while prediction ensembling contributes only 0.33 dB.

### 5.2. Masking Ratio

In Table 6, we present the effects of different masking ratios when training the denoiser with AWGN. A low masking ratio fails to bridge the gap between the training and testing distributions, leading to overfitting.

### 5.3. Iterative Noise Sampler Boosting

In Table 3, we demonstrate the effect of our iterative boosting of the denoiser by reporting the PSNR of our denoiser after in each round. We observe that its performance gradually improves before eventually stagnating, with no further gains observed.

### 5.4. Denoiser Network Architecture

In Table 2, we present a comparison of the network architecture of our denoiser. With a more powerful network such as NAFNet [5], we achieve better results. This suggests that our method could benefit from an improved network architecture.

### 5.5. Prediction Ensemble Set Size $K$

In Table 5, we present the effect of the number of predictions used in our ensemble. Ensembling multiple predictions improves the denoising performance, and it almost saturates with  $K = 10$ .

## 6. Conclusions

In this work, we propose a novel approach to solving real-world image unsupervised denoising eliminating the need for adversarial training and its associated limitations. We introduce a new method for integrating random masking to train a denoiser in a supervised manner, by allowing it to jointly denoise and inpaint images corrupted by noise. We iteratively improve our noise sampler by leveraging the denoiser’s predictions and a dataset of real noise images. We demonstrate that MID achieves state-of-the-art performance in unsupervised real-world image denoising.



## References

- [1] Abdelrahman Abdelhamed, Stephen Lin, and Michael S. Brown. A high-quality denoising dataset for smartphone cameras. In *IEEE Conference on Computer Vision and Pattern Recognition (CVPR)*, 2018. 6
- [2] Jian-Feng Cai Bao, Chenglong and Hui Ji. Fast sparsity-based orthogonal dictionary learning for image restoration. In *Proceedings of the IEEE International Conference on Computer Vision*, 2013. 2
- [3] Bartomeu Coll Buades Antoni and Jean-Michel Morel. Non-local means denoising. In *Image Processing On Line 1*, 2011. 2
- [4] Harold C Burger, Christian J Schuler, and Stefan Harmeling. Image denoising: Can plain neural networks compete with bm3d? In *2012 IEEE conference on computer vision and pattern recognition*, pages 2392–2399. IEEE, 2012. 2
- [5] Liangyu Chen, Xiaojie Chu, Xiangyu Zhang, and Jian Sun. Simple baselines for image restoration. In *European conference on computer vision*, pages 17–33. Springer, 2022. 6, 8
- [6] Shiyang Chen, Jiyuan Zhang, Zhaofei Yu, and Tiejun Huang. Exploring efficient asymmetric blind-spots for self-supervised denoising in real-world scenarios. In *Proceedings of the IEEE/CVF Conference on Computer Vision and Pattern Recognition*, pages 2814–2823, 2024. 3, 7, 8
- [7] Kostadin Dabov, Alessandro Foi, Vladimir Katkovnik, and Karen Egiazarian. Bm3d image denoising with shape-adaptive principal component analysis. In *SPARS'09-Signal Processing with Adaptive Sparse Structured Representations*, 2009. 2, 7
- [8] Jia Deng, Wei Dong, Richard Socher, Li-Jia Li, Kai Li, and Li Fei-Fei. Imagenet: A large-scale hierarchical image database. In *2009 IEEE conference on computer vision and pattern recognition*, pages 248–255. Ieee, 2009. 3
- [9] Michael Elad, Bahjat Kawar, and Gregory Vaksman. Image denoising: The deep learning revolution and beyond – a survey paper –, 2023. 1
- [10] Jang Geonwoon, Lee Wooseok, Son Sanghyun, and Lee Kyoung Mu. C2n: Practical generative noise modeling for real-world denoising. In *Proceedings of the IEEE/CVF International Conference on Computer Vision*, pages 2350–2359, 2021. 3, 7, 8
- [11] Shuhang Gu, Lei Zhang, Wangmeng Zuo, and Xiangchu Feng. Weighted nuclear norm minimization with application to image denoising. In *Proceedings of the IEEE conference on computer vision and pattern recognition*, pages 2862–2869, 2014. 7
- [12] Alexander Krull, Tim-Oliver Buchholz, and Florian Jug. Noise2void-learning denoising from single noisy images. In *Proceedings of the IEEE/CVF conference on computer vision and pattern recognition*, pages 2129–2137, 2019. 2
- [13] Alexander Krull, Tomáš Vičar, Mangal Prakash, Manan Lalit, and Florian Jug. Probabilistic noise2void: Unsupervised content-aware denoising. *Frontiers in Computer Science*, 2:5, 2020. 2
- [14] Alina Kuznetsova, Hassan Rom, Neil Alldrin, Jasper Uijlings, Ivan Krasin, Jordi Pont-Tuset, Shahab Kamali, Stefan Popov, Matteo Mallocci, Alexander Kolesnikov, et al. The open images dataset v4: Unified image classification, object detection, and visual relationship detection at scale. *International journal of computer vision*, 128(7):1956–1981, 2020. 3
- [15] Samuli Laine, Tero Karras, Jaakko Lehtinen, and Timo Aila. High-quality self-supervised deep image denoising. *Advances in Neural Information Processing Systems*, 32, 2019. 2
- [16] Wooseok Lee, Sanghyun Son, and Kyoung Mu Lee. Apbsn: Self-supervised denoising for real-world images via asymmetric pd and blind-spot network. In *Proceedings of the IEEE/CVF Conference on Computer Vision and Pattern Recognition*, pages 17725–17734, 2022. 2, 7
- [17] Junyi Li, Zhilu Zhang, Xiaoyu Liu, Chaoyu Feng, Xiaotao Wang, Lei Lei, and Wangmeng Zuo. Spatially adaptive self-supervised learning for real-world image denoising. In *Proceedings of the IEEE/CVF Conference on Computer Vision and Pattern Recognition*, pages 9914–9924, 2023. 3, 7
- [18] Tsung-Yi Lin, Michael Maire, Serge Belongie, James Hays, Pietro Perona, Deva Ramanan, Piotr Dollár, and C Lawrence Zitnick. Microsoft coco: Common objects in context. In *Computer Vision—ECCV 2014: 13th European Conference, Zurich, Switzerland, September 6-12, 2014, Proceedings, Part V 13*, pages 740–755. Springer, 2014. 3
- [19] Xin Lin, Chao Ren, Xiao Liu, Jie Huang, and Yinjie Lei. Unsupervised image denoising in real-world scenarios via self-collaboration parallel generative adversarial branches. In *Proceedings of the IEEE/CVF International Conference on Computer Vision*, pages 12642–12652, 2023. 1, 3, 7, 8, 12
- [20] Elad Michael and Michal Aharon. Image denoising via sparse and redundant representations over learned dictionaries. In *IEEE Transactions on Image processing 15.12*, 2006. 2
- [21] Reyhaneh Neshatavar, Mohsen Yavartanoo, Sanghyun Son, and Kyoung Mu Lee. Cvf-sid: Cyclic multi-variate function for self-supervised image denoising by disentangling noise from image. In *Proceedings of the IEEE/CVF Conference on Computer Vision and Pattern Recognition*, pages 17583–17591, 2022. 2, 7
- [22] Yizhong Pan, Xiao Liu, Xiangyu Liao, Yuanzhouhan Cao, and Chao Ren. Random sub-samples generation for self-supervised real image denoising. In *Proceedings of the IEEE/CVF International Conference on Computer Vision*, pages 12150–12159, 2023. 1, 3, 7, 12
- [23] Tobias Plotz and Stefan Roth. Benchmarking denoising algorithms with real photographs. In *Proceedings of the IEEE conference on computer vision and pattern recognition*, pages 1586–1595, 2017. 6
- [24] Olaf Ronneberger, Philipp Fischer, and Thomas Brox. U-net: Convolutional networks for biomedical image segmentation. In *International Conference on Medical image computing and computer-assisted intervention*, pages 234–241. Springer, 2015. 7
- [25] Gu S., Zhang L., and X. Zuo W. & Feng. Weighted nuclear norm minimization with application to image denoising. In *In Proceedings of the IEEE conference on computer vision and pattern recognition*, 2014. 2

- [26] Hossein Talebi and Peyman Milanfar. Global image denoising. *IEEE Transactions on Image Processing*, 23(2):755–768, 2013. [2](#)
- [27] Zejin Wang, Jiazheng Liu, Guoqing Li, and Hua Han. Blind2unblind: Self-supervised image denoising with visible blind spots. In *Proceedings of the IEEE/CVF Conference on Computer Vision and Pattern Recognition*, pages 2027–2036, 2022. [2](#)
- [28] Zichun Wang, Ying Fu, Ji Liu, and Yulun Zhang. Lg-bpn: Local and global blind-patch network for self-supervised real-world denoising. In *Proceedings of the IEEE/CVF Conference on Computer Vision and Pattern Recognition*, pages 18156–18165, 2023. [3](#), [7](#)
- [29] Xiaohe Wu, Ming Liu, Yue Cao, Dongwei Ren, and Wangmeng Zuo. Unpaired learning of deep image denoising. In *European conference on computer vision*, pages 352–368. Springer, 2020. [3](#), [7](#), [8](#)
- [30] Zongsheng Yue, Hongwei Yong, Qian Zhao, Deyu Meng, and Lei Zhang. Variational denoising network: Toward blind noise modeling and removal. *Advances in neural information processing systems*, 32, 2019. [2](#), [7](#)
- [31] Syed Waqas Zamir, Aditya Arora, Salman Khan, Munawar Hayat, Fahad Shahbaz Khan, and Ming-Hsuan Yang. Restormer: Efficient transformer for high-resolution image restoration. In *Proceedings of the IEEE/CVF conference on computer vision and pattern recognition*, pages 5728–5739, 2022. [2](#), [7](#)
- [32] Kai Zhang, Wangmeng Zuo, Yunjin Chen, Deyu Meng, and Lei Zhang. Beyond a gaussian denoiser: Residual learning of deep cnn for image denoising. *IEEE transactions on image processing*, 26(7):3142–3155, 2017. [2](#), [7](#), [8](#)
- [33] Lei Zhang, Weisheng Dong, David Zhang, and Guangming Shi. Two-stage image denoising by principal component analysis with local pixel grouping. *Pattern recognition*, 43(4):1531–1549, 2010. [2](#)
- [34] Maria Zontak, Inbar Mosseri, and Michal Irani. Separating signal from noise using patch recurrence across scales. In *proceedings of the IEEE conference on computer vision and pattern recognition*, pages 1195–1202, 2013. [2](#)

## A. Impact of masking on the train-test distribution gap

we show that masking reduces the distribution gap between the original training and testing inputs.

**Proposition 1.** *Let  $a^s = \mathbf{M} \odot y^s$  and  $b^s = (1 - \mathbf{M}) \odot y^s$  be the visible and hidden pixels of a synthetic noisy image, and  $a^r = \mathbf{M} \odot y^r$  and  $b^r = (1 - \mathbf{M}) \odot y^r$  be the visible and hidden pixels of a real noisy image, respectively. Let us also denote with  $p(a, b)$  the probability density function of synthetic data  $y^s$  and with  $q(a, b)$  the probability density function of real data  $y^r$ , where  $a$  and  $b$  are the visible and hidden entries of the images, respectively. Then,  $D_{\text{KL}}(p(a, b) \| q(a, b)) \geq D_{\text{KL}}(p(a) \| q(a))$ , where  $D_{\text{KL}}(p \| q)$  denotes the Kullback-Leibler divergence between  $p$  and  $q$ .*

*Proof.* By using Bayes rule we have

$$\begin{aligned} D_{\text{KL}}(p(a, b) \| q(a, b)) &= \\ \int p(a) D_{\text{KL}}(p(b|a) \| q(b|a)) da + D_{\text{KL}}(p(a) \| q(a)) &= \\ &\geq D_{\text{KL}}(p(a) \| q(a)), \end{aligned}$$

since  $p(a) \geq 0$  and also  $D_{\text{KL}}(p(b|a) \| q(b|a)) \geq 0$ .  $\square$

## B. Additional qualitative comparison

We provide an additional qualitative comparison on the SIDD validation dataset in Figure 7. We can see visually that MID tends to output restored images with texture at a higher level of detail and while reducing noise more than other unsupervised methods.

## C. Efficiency comparison

We provide an efficiency comparison in Table 7. For a fair comparison with AT-BSN, which is a distillation method, we distill our model using the network they used and denote this method as Ours(distilled). Our vanilla method maintains reasonable efficiency, while our distilled version outperforms AT-BSN.

Table 7. Performance/efficiency trade-off on SIDD validation.

Method	SCPGabNet	AT-BSN	Ours(K=10)	Ours(distilled)
Time (ms)	<u>62</u>	<b>32</b>	201	<b>32</b>
PSNR (dB)	36.53	37.88	<b>38.05</b>	<u>37.96</u>

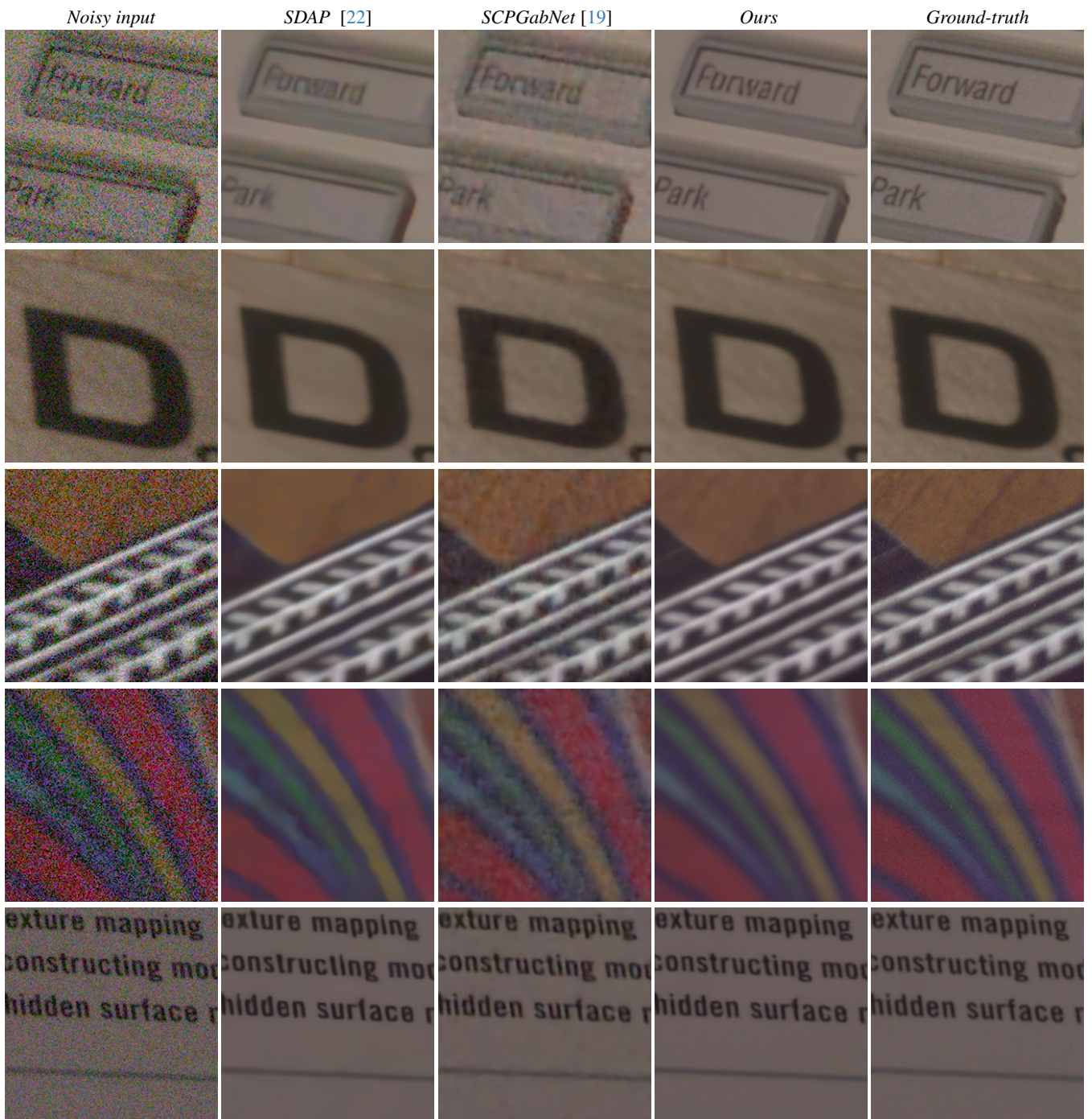


Figure 7. Visual comparison on SIDD validation dataset. Zooming in is recommended to see the differences in reconstruction accuracy.